



**HAL**  
open science

# Investigation of single bubbles rising in Newtonian and non-Newtonian fluids inside a thin-gap bubble column intended for microalgae cultivation

Sikandar Almani, Walid Blel, Emilie Gadoin, Caroline Gentric

## ► To cite this version:

Sikandar Almani, Walid Blel, Emilie Gadoin, Caroline Gentric. Investigation of single bubbles rising in Newtonian and non-Newtonian fluids inside a thin-gap bubble column intended for microalgae cultivation. *Chemical Engineering Research and Design*, 2021, 167, pp.218-230. 10.1016/j.cherd.2021.01.010 . hal-04225123

**HAL Id: hal-04225123**

**<https://nantes-universite.hal.science/hal-04225123>**

Submitted on 2 Oct 2023

**HAL** is a multi-disciplinary open access archive for the deposit and dissemination of scientific research documents, whether they are published or not. The documents may come from teaching and research institutions in France or abroad, or from public or private research centers.

L'archive ouverte pluridisciplinaire **HAL**, est destinée au dépôt et à la diffusion de documents scientifiques de niveau recherche, publiés ou non, émanant des établissements d'enseignement et de recherche français ou étrangers, des laboratoires publics ou privés.



Distributed under a Creative Commons Attribution 4.0 International License

## Investigation of single bubbles rising in Newtonian and non-Newtonian fluids inside a thin-gap bubble column intended for microalgae cultivation

Sikandar Almani<sup>1,2</sup>, Walid Blel<sup>1</sup>, Emilie Gadoin<sup>1</sup>, Caroline Gentric<sup>1\*</sup>

<sup>1</sup>Université de Nantes, CNRS, GEPEA, UMR 6144 F-44600 Saint-Nazaire, France.

<sup>2</sup>Department of Chemical Engineering, Mehran University of Engineering and Technology, Jamshoro, Pakistan

### Abstract

Single bubbles rising in a confined geometry – a parallelepipedic bubble column with a 4 mm thickness - in the presence of a non-Newtonian liquid phase are studied using a shadowgraphy technique. The context is the cultivation of microalgae at high cell concentrations. **In fact**, it necessitates the reduction of the bioreactor thickness to allow light penetration through the whole culture. **In the same time**, the medium becomes shear-thinning for biomass concentrations higher than 30 g·L<sup>-1</sup>. A 2 g·L<sup>-1</sup> **carboxymethyl cellulose (CMC)** and a 1 g·L<sup>-1</sup> **Xanthan Gum (XG)** aqueous solutions are studied to mimic the behavior of 42 g·L<sup>-1</sup> *Chlorella vulgaris* cultures. **Besides**, a comparison with water, representing the Newtonian liquid phase at low culture concentrations, is proposed. The bubble equivalent diameter is varied between 1.34 and 3.36 mm using different capillary sizes to generate the bubbles. Results show the complex and coupled effects of confinement and shear-thinning behavior of the liquid phase on bubbles terminal velocity, shape and trajectory. In fact, compared to the case of an infinite liquid medium, confinement increases wall friction on the bubbles, while reduces the liquid phase apparent viscosity in its neighborhood due to increased shear rate. This is why, depending on the bubble size, the bubble terminal velocity in shear-thinning fluids can be higher or lower than in unconfined conditions. For bubbles rising in shear-thinning fluids,

---

\*Corresponding author; C. Gentric, E-mail address: [caroline.gentric@univ-nantes.fr](mailto:caroline.gentric@univ-nantes.fr)

contrary to water, it is observed that confinement induces a transition from spherical shape to ellipsoidal shape that occurs sooner in terms of bubbles diameter or Eo number. A correlation for the bubble drag coefficient in confined conditions in presence of shear-thinning fluids is also proposed for confinement ratios  $d_b/e$  between 0.34 and 0.84.

**Keywords:** thin-gap bubble column, non-Newtonian liquid, single bubble terminal velocity, drag coefficient.

## 1. Introduction

Interactions between gas and liquid phases are essential to perform a variety of chemical and biochemical reactions in process industries. There are many different reactor types, which are used for this purpose such as packed column, bubble column, spray tower, gas-liquid agitated vessel etc...The design and scale-up of a bubble column reactor require a complete understanding of its complex hydrodynamics, which is mainly influenced by the physical properties of the phases (Akita and Yoshida, 1973; Esmaeili et al., 2015; Loubière and Hébrard, 2004; Thobie et al., 2017), the operating conditions (Letzel et al., 1999; Vial et al., 2000) and the design parameters (Kumar and Vanka, 2015; Ruzicka et al., 2001; Sharaf et al., 2016).

Photobioreactors (PBRs) dedicated to the culture of microalgae or cyanobacteria are a promising technology for numerous applications such as the production of high value-added products, of bioenergy or for CO<sub>2</sub> capture. For this purpose, optimization of culture parameters and PBR design are two possible solutions in order to obtain high volumetric productivities, reduce production costs and environmental impacts and to increase energy efficiency. In this context, intensification of performances via an increase of culture concentration for a given illuminated surface represents a promising way to achieve optimized and eco-efficient production.

The intensified PBR configuration used in this study consists in a thin-gap bubble column (4 mm gap) expected to allow cultivating high biomass concentration while ensuring light availability on the whole reactor thickness (Souliès, 2014). Compared to conventional bubble columns, with a thickness of a few centimeters, it is shown that confinement results in a high change of hydrodynamics and mass transfer (Thobie et al., 2017). Added to this, when the biomass concentration increases, an increase of the continuous phase viscosity first appears and then a non-Newtonian behavior is observed (Souliès et al., 2013).

More precisely, concerning the rheological behavior of concentrated microalgae solutions of *Chlorella vulgaris*, Souliès et al. (2013) observed that the behavior remains Newtonian until a dry biomass concentration of  $30 \text{ g}\cdot\text{L}^{-1}$  which corresponds to a cell volume fraction of 0.115. In this domain, the viscosity increases with the cell volume fraction following the Quemada model (Quemada, 1977) commonly used to estimate the viscosity of concentrated suspensions. For higher values of the cell volume fraction, between 0.115 and 0.25, the rheological behavior becomes shear thinning, whereas for the highest volume fractions ( $> 0.25$ ), an apparent yield stress regime is observed. The same shear-thinning behavior is observed for other strains at high cell concentrations: *Chlamydomonas reinhardtii* by Rafai et al. (2010), *Nannochloris sp.* and *Chlorella vulgaris* by Wileman et al. (2012) and *Scenedesmus obliquus* by Adesanya et al. (2012). These changes in the liquid phase properties will impact PBR hydrodynamics. In fact, increase in liquid phase viscosity and rheology modification favor bubbles coalescence and reduce the homogeneous regime range in bubble columns (Fransolet et al., 2005; Jamshidi and Mostoufi, 2018).

In PBR technology, mixing is ensured by bubbling and is essential to avoid inorganic carbon and nutrient local limitation, but also to avoid pH and temperature gradients and to prevent cell sedimentation. Another important role of mixing is to ensure that cells are regularly exposed to light. Bubbles have also a key role in the gas-liquid mass transfer which has to be

sufficient to prevent both carbon limitation by absorption of injected CO<sub>2</sub> and oxygen inhibition by stripping of produced O<sub>2</sub> (Thobie et al., 2017). To better understand the bubbling effect on flow pattern as well as mixing and mass transfer in confined geometries in the presence of a non-Newtonian liquid phase, experimental investigations have first to be carried out to characterize the physical phenomena governing the rising of single bubbles.

Study of single bubbles rising in non-Newtonian liquids has now been investigated by a few authors (see for instance the synthesis of Chhabra (2006)) and correlations for bubble terminal velocities or drag coefficients of bubbles in infinite non-Newtonian liquid media can be found in the literature (Dewsbury et al., 1999; Fan et al., 2014; Margaritis et al., 1999). In this context, the power-law model to describe the rheological behavior has received most of the attention.

Effect of confinement in 2D thin-gap bubble columns has been reported for isolated bubbles in Newtonian liquids: Figueroa-Espinoza et al.(2008) reported the effect of the confinement ratio (ratio between bubble radius and gap width) and Re number (range 30-500) on the bubble drag coefficient and identified two regimes depending on bubbles having rectilinear or oscillating paths. Roig et al.(2012) have carried out a complete study, by shadowgraphy and PIV, of a single bubble rising in a 1 mm Hele-Shaw cell over a wide range of Re (50-6000), they identified several regimes as far as the bubble trajectory, wake and shape are concerned. Filella et al. (2015) extended the study of Roig et al.(2012) by characterizing the movement of a single bubble in 3 mm Hele-Shaw cell; among others, they proposed a scaling law for the terminal velocity of highly confined bubbles ( $d_b/e > 1.4$ , where  $e$  is the gap width and  $d_b$  the bubble diameter). Recently, Hashida et al. (2019) investigated the effect of confinement ratio ( $2.3 \leq d_b/e \leq 6.7$ ) and viscosity (from 0.9 to 65.7 mPa·s) on the bubble velocity, shape and trajectory in highly confined conditions. Gumulya et al. (2021) carried out a complete numerical study to investigate the effect of confinement on bubble shape, trajectory,

oscillations and wake velocity field. Some other studies investigated the impact of confinement on the mass transfer around a single bubble, using planar laser induced turbulence (Roudet et al., 2017), UV induced turbulence (Zhang et al., 2020) or a colorimetric method ((Kherbeche et al., 2020)(Felis et al., 2019)).

But, to our knowledge, studies dealing with isolated bubbles rising in non-Newtonian fluids within confined geometries are extremely rare. Böhm et al. (2014) investigated the behavior of bubbles with diameters between 3 and 9 mm ascending in 2D columns with a depth of 5 or 7 mm; they compared the presence of non-Newtonian fluid - a XG solution – as the continuous phase to the case of water. Their goal was to reach a better understanding of the phenomena involved in flat sheet membrane bioreactors which operate as airlift gas-liquid reactors; the XG solution mimics the activated sludge that is filtered in membrane bioreactors. They put into evidence the influence of the column depth and the bubble size on the rising path, the bubble shape, the terminal velocity and bubble oscillations. In another paper, the same authors analyzed the liquid velocity field around the bubble using PIV (Böhm et al., 2016), and the shear stress induced by the bubble passage thanks to the electro-diffusion method, in fact this shear stress can help cleaning the deposition layer at the membrane surfaces (Böhm et al., 2013).

In the present study, the effect of confinement on the rising behavior of an isolated bubble generated in a thin-gap bubble column (4 mm thickness) which can be used as intensified PBR (Thobie et al., 2017) is analyzed experimentally. To mimic the shear-thinning behavior of *Chlorella vulgaris* cultures at concentrations of around  $42 \text{ g}\cdot\text{L}^{-1}$  (volume fraction  $\Phi_v = 0.167$ ) (Souliès et al., 2013), solutions of XG and CMC are used respectively at the concentrations of  $1 \text{ g}\cdot\text{L}^{-1}$  and  $2 \text{ g}\cdot\text{L}^{-1}$ . In order to put forward the effect of viscosity and shear-thinning, demineralized water is also used as a Newtonian fluid. Five different capillary

diameters ( $d_{cap}$ ) allow to generate bubbles with different equivalent diameters ( $d_b$ ). Bubbles are only slightly confined with confinement ratio  $d_b/e$  varying between 0.34 and 0.84.

Bubble velocities, shapes and trajectories are characterized by shadowgraphy. Special attention is paid to terminal velocity ( $V_t$ ) which governs the contact time between the bubbles and the surrounding liquid and thus the gas-liquid mass transfer coefficient (Higbie, 1935). Results are compared to literature ones available for infinite liquid medium to put forward the specific hydrodynamics induced by the confinement and the rheological behavior. Based on dimensional analysis, an empirical correlation is also proposed for the drag coefficient of single bubbles rising steadily in stagnant power-law liquids in thin-gap columns.

## 2. Materials and methods

### 2.1. Fluids characterization and properties

In this study, non-Newtonian solutions are used to mimic as close as possible the shear-thinning behavior of *Chlorella Vulgaris* cultures at high concentration ( $42 \text{ g}\cdot\text{L}^{-1}$ ) (Souliès et al., 2013). For this purpose, aqueous solutions of CMC at  $2 \text{ g}\cdot\text{L}^{-1}$  (BDH) and of XG at  $1 \text{ g}\cdot\text{L}^{-1}$  (Sigma-Aldrich) were considered as non-Newtonian fluids. They were prepared by dissolving the appropriate amount of polymers in demineralized water for one day with continuous agitation. Demineralized water was used as a reference Newtonian fluid.

The rheological characterization of these model fluids was performed at  $22^\circ\text{C}$  using a rotational stress-controlled rheometer (MCR500, PAAR Physica®) equipped with a cone-plate device (50 mm in diameter, 3 degrees in cone angle). The shear rate was varied in the range of  $0.01\text{-}1000 \text{ s}^{-1}$ . At the tested concentrations, CMC and XG solutions present a rheological behavior close to the one of *Chlorella Vulgaris* at  $42 \text{ g}\cdot\text{L}^{-1}$ . The power-law model is used to represent the shear-thinning behavior of these CMC and XG solutions:

$$\tau = K \cdot \dot{\gamma}^n \quad 0 < n < 1 \quad (1)$$

where  $\tau$  is the shear stress and  $\dot{\gamma}$  the shear rate. The power law parameters are the consistency index  $K$  and the flow index  $n$  which is lower than one for shear-thinning fluids. For power law fluids, the dynamic viscosity, used for Newtonian fluids, is thus replaced by the apparent viscosity,  $\mu_{app}$ :

$$\mu_{app} = K \cdot \dot{\gamma}^{n-1} \quad (2)$$

The surface tensions of the CMC and XG solutions have been analyzed using the pendant drop method (Krüss-DSA30 Drop Shape Analyzer). The densities of the solutions have been determined using a gravity hydrometer (Fisher Scientific). The rheological and physicochemical properties of the studied Newtonian and non-Newtonian fluids are presented in Table 1.

**Table 1:** Physico-chemical and rheological properties of Newtonian and non-Newtonian fluids

Fluids	$\rho$ (kg·m <sup>-3</sup> )	$\sigma$ (N·m <sup>-1</sup> )	$K$ (Pa·s <sup>n</sup> )	$n$	$T$ (°C)
Demineralized water	1000	0.0728 ± 0.002	0.0010	1.00	22
2 g·L <sup>-1</sup> CMC solution	1001.3	0.0674 ± 0.001	0.0608	0.649	22
1 g·L <sup>-1</sup> XG solution	998.7	0.0519 ± 0.002	0.200	0.396	22
<i>Chlorella Vulgaris</i> suspension (42 g·L <sup>-1</sup> )			0.0561	0.311	22

## 2.2. Experimental set-up

Bubble rising characterization is carried out in a thin-gap parallelepipedic bubble column (4 x 300 x 1200 mm<sup>3</sup>, unaerated liquid level of 1000 mm) made with transparent PMMA (polymethyl methacrylate) (Figure 1). Gas injection can be performed through capillaries of different diameters:  $d_{cap} = 0.127, 0.254, 0.508, 0.762$  or  $1.016$  mm located at the bottom of the column. These capillaries are used to generate bubbles with different diameters at low frequency with the help of a low-pressure syringe pump (neMESYS-NEM-B101-02B).

The gas injection procedure consists in setting a flowrate of gas using the interface of the syringe pump. Several gas flowrates have been tested: the flowrate has to be low enough in

order to have bubbles sufficiently distant to avoid any bubble - bubble interaction which could distort the measured value of the terminal velocity, but it has to be high enough to allow to characterize a sufficient number of bubbles to obtain a statistically consistent estimation of the terminal velocity in a reasonable amount of time (see paragraph 2.3).

The shadowgraphy measurement zone ( $80 \times 108 \text{ mm}^2$ ) is located at a height of 540 mm from the bottom of column. This position, corresponding to the mid-height of the column, was chosen to make sure that bubbles have reached their terminal velocity. The capillary is positioned at 7 cm from the lateral wall. This distance is considered sufficient to avoid wall influence on the hydrodynamics of isolated bubbles (van Sint Annaland et al., 2005).

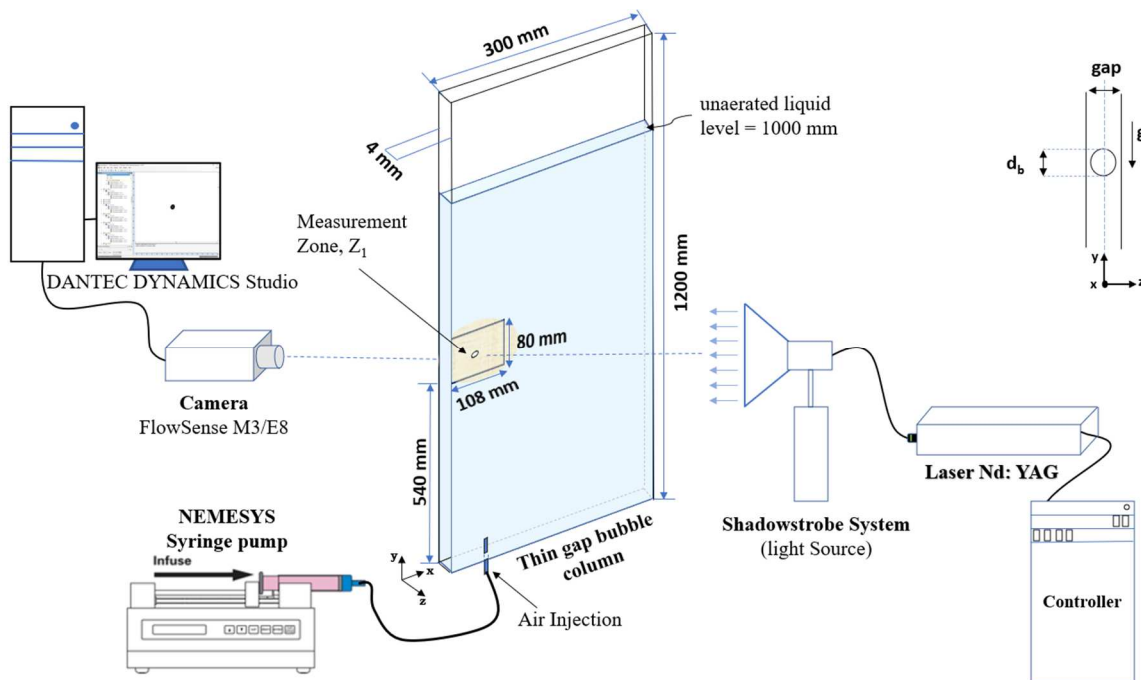


**Figure 1:** Experimental set-up for the investigation of isolated bubble rising

### 2.3. Shadowgraphy measurements

Size, shape and instantaneous velocity of the bubbles are measured using a shadowgraphy method. It is an optical flow visualization technique that involves placing the fluid to be studied between the light source and a light-receiving sensor. DANTEC DYNAMICS ShadowStrobe system is used in this study. This system consists of a Nd-YAG pulsed laser

used to illuminate an optical fiber providing extremely short light pulses from a few nanoseconds to hundreds of nanoseconds. For uniform illumination, the shadowstrobe system and the camera are aligned in the same optical axis. The camera (FlowSense M3/E8) is used to record images at the pulsation frequency set by the lighting system and using a synchronization system. The camera has a resolution of 1600 x 1186 pixels and is equipped with a fixed focal lens of 60 mm with a variable aperture from 2.3 to 32 and a maximum frequency of 15 Hz. During all acquisitions, the imaging frequency is taken at its maximum value. This type of measurement is possible in our confined column case since bubbles are always in the same plane. This technique is suitable for bubbles for which the light rays passing through the edge of the bubble are deflected causing a shadow area to appear. In a similar earlier study (Roudet, 2008), images of very sharp confined bubbles were observed with a well-defined visualization of the contour. Figure 1 also presents the measuring devices related to shadowgraphy.

For each detected bubble, the image analysis software estimates the projected area in a vertical plane. Then the equivalent diameter ' $d_b$ ' corresponds to the diameter of a spherical bubble having the same projected area as the measured bubble (Thobie et al., 2017).

The horizontal and vertical components of the bubble velocity (respectively  $u$  and  $v$ ) are determined as the horizontal and vertical displacements of the gravity center between two frames divided by the time between two laser pulses. Then, only the vertical component of the velocity of the single bubble rising in the column is considered for the determination of terminal velocity. In order to determine accurately the terminal velocity of the bubbles generated by each capillary in a given fluid, the following procedure has been applied for increasing air flowrates:

- For each tested capillary and for a given syringe flowrate, velocities obtained from several images (Figure 2a) are averaged, the number of measurements (blue points in Figure 2b) has to be sufficient to obtain a constant cumulative average velocity (red line in Figure 2b),
- For each capillary, the cumulative average velocities are plotted vs the syringe flowrate (Figure 2c); the deviation in the velocity which appears above a critical flowrate is due to the interaction between the studied bubble and the wake of the upstream one, since the distance between the bubbles decreases when the flowrate increases.
- The similar velocities – obtained below the critical flowrate - are then averaged and considered as the terminal velocity for each tested capillary (dashed red line in Figure 2c). The standard deviation is calculated from all the instantaneous velocities that led to these similar velocities.

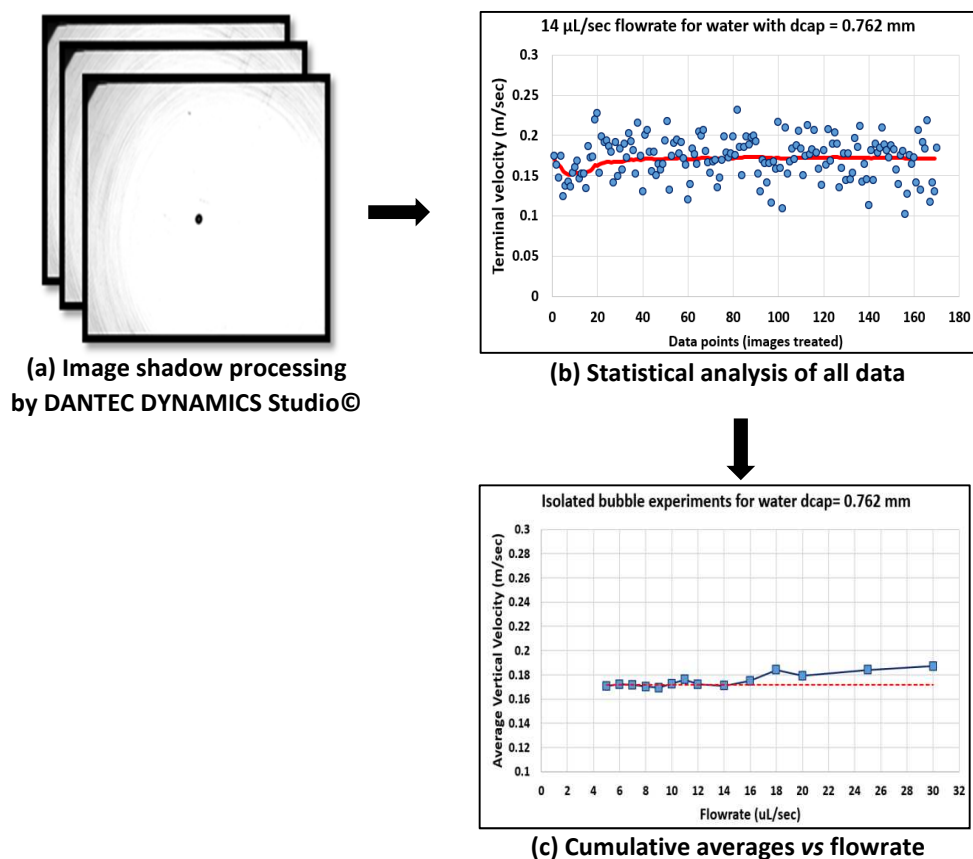


**Figure 2:** Experimental determination of the terminal velocity of isolated bubbles

### 3. Results and discussion

#### 3.1. Terminal velocity of isolated bubbles in 2D confined conditions

This paragraph presents the experimental terminal velocities of single bubbles ascending in the thin-gap parallelepipedic bubble column described in paragraph 2.2. In this configuration, the confinement ratio remains lower than 1:  $0.34 < d_b/e < 0.84$ , which corresponds to an intermediate domain between complete confinement where bubble are flattened ( $d_b/e > 1$ ) and an infinite liquid medium. Table 2 gives the values of the terminal velocities obtained for different capillary diameters and in 3 liquids (water, CMC and XG aqueous solutions). The bubble diameters obtained under the tested conditions are between 1.34 and 3.36 mm. Results are compared to literature ones - when available - for infinite medium in Newtonian (correlation of Jamialahmadi et al. (1994)) and non-Newtonian (experimental results of Margaritis et al.(1999)) liquids. The objective is to put forward the specific hydrodynamics induced by confinement and liquid rheology on the bubble rise in the column.

The comparison between terminal velocities in water on one side, and in CMC and XG solutions on the other side, shows higher velocities in water, which highlights the impact of the viscosity and rheological behavior of the continuous phase on the bubble rise in the column. The same behavior was observed in unconfined columns: for instance, Islam et al. (2020) reported **bubble terminal velocities** decreasing with increasing Morton numbers via numerical simulations.

Figure 3(a) shows the evolution of the terminal velocity *vs* the diameter for isolated bubbles rising in demineralized water. A comparison with the values for an infinite medium (Jamialahmadi et al.,(1994) and Clift et al., (1978)) is presented. The same decrease of  $V_t$  with  $d_b$  is observed for bubble diameters between 1.74 mm and 3.12 mm, but with lower terminal velocities in the confined column. A sudden increase is observed for the 3.28 mm diameter, which is not observed in the case of an infinite medium. In their study carried out in thin

columns with a 5 or 7 mm gap, Böhm et al. (2014) also observed a decrease followed by an increase of the bubble terminal velocity as a function of the diameter, the transition occurring for a higher diameter, *i.e.* 5 mm, but a quantitative comparison with the present case is not possible since the confinement ratio is different in both studies. Globally, the comparison with literature results for an infinite medium (Jamialahmadi et al., 1994) shows that, due to increased wall friction, confinement decreases significantly the terminal velocity of the bubbles **in water**, with a ratio of confined to unconfined velocities varying between 0.6 and 0.8 (Table 2).

**Figure 3(b)** presents the evolution of bubble terminal velocities *vs* diameter in non-Newtonian fluids. Two domains are observed depending on the bubble diameter. In a first domain, *i.e.* for small bubble diameters up to 2.2 mm, the terminal velocity increases with the diameter, and for diameters greater than 2.2 mm, a plateau of terminal velocity appears. Figure 3(b) also presents the terminal velocity evolution as measured by Margaritis et al.(1999) for solutions of XG at the same concentration of  $1 \text{ g}\cdot\text{L}^{-1}$  in an unconfined geometry. They observed the same type of evolution (increase followed by a plateau) but with the plateau appearing at a higher diameter (around 5 mm). They also worked with CMC solutions, but it must be noted that the lowest concentration of CMC they tested is  $3.74 \text{ g}\cdot\text{L}^{-1}$ , while in our case a concentration of  $2 \text{ g}\cdot\text{L}^{-1}$  is used. Since these authors noticed that the diameter at which the plateau appears increases with the polysaccharide concentration, but that the plateau level is independent of the concentration, only their plateau value is reported in Figure 3(b) for CMC.

In fact, Margaritis et al. (1999) investigated bubble rise velocities in several polysaccharide solutions and observed that the terminal velocity is proportional to the bubble volume in log scale at the lowest volumes (creeping flow regime) and reaches a plateau for the highest ones. This tendency is observed whatever the polysaccharide solution and its concentration. For CMC (concentration  $> 3.74 \text{ g}\cdot\text{L}^{-1}$ ) and XG solutions (concentration  $> 0.36 \text{ g}\cdot\text{L}^{-1}$ ), their plateau

of terminal velocity corresponds to values of  $24 \text{ cm}\cdot\text{s}^{-1}$  and  $27 \text{ cm}\cdot\text{s}^{-1}$  respectively. For the thin gap bubble column, a similar evolution of the terminal velocity vs the diameter is observed. However, the linear evolution in log scale is observed only up to bubble diameters of 2.2 mm, with higher terminal velocity values than in unconfined column for the same bubble diameter in the  $1 \text{ g}\cdot\text{L}^{-1}$  XG solution. From this position, the plateau of terminal velocity is installed at a level lower than the one in an infinite medium, *i.e.* at 16 cm/s and 18 cm/s respectively for XG and CMC.

The influence of confinement on the terminal velocity is different in shear-thinning fluids and in water: indeed, for a bubble of diameter lower than 2.2 mm rising in a confined medium in XG solution ( $1 \text{ g}\cdot\text{L}^{-1}$ ), the terminal velocity is 1.254 - 1.342 times higher than in **infinite liquid**, whereas for the bubble diameters greater than 3 mm the terminal velocity is 0.722 to 0.918 times lower in comparison to the experimental values of Margaritis et al. (1999) (Table 2). Therefore, contrary to what is observed for water, in non-Newtonian solutions, confinement does not always reduce the terminal velocity. This result can be explained by antagonistic effects, in confined conditions, of the wall friction on one side and of the shear-thinning behavior of non-Newtonian polysaccharide solutions (CMC and XG) on the other side. Indeed, confined conditions induce an increase in wall friction which tends to decrease the bubble velocity as observed for water. But at the same time, **they increase** the shear rate **between the bubble and the walls** which induces lower viscosity for the shear-thinning solutions and thus tends to increase the bubble velocity compared to an infinite medium. Here the effect of shear-thinning outweighs the one of confinement at the lowest bubble diameters - ***i.e.* the lowest confinement ratios: for  $d_b \leq 2.2 \text{ mm}$  corresponding to  $d_b/e \leq 0.55$**  - since the terminal velocity in confined conditions is higher than in infinite liquid medium. **For the largest bubble diameters, *i.e.* the highest confinement ratios, the wall friction effect dominates with a smaller terminal velocity in confined conditions.** The same antagonistic effects were

already described by Böhm et al. (2014) with thin-gap bubble columns of 5 and 7 mm of thickness, even in their case, the experimental terminal velocity was always lower in confined conditions. Direct comparison with the experiments of Böhm et al. (2014) is not possible since their column gap is different, and at the exception of one measurement, their confinement ratio is always higher than in the present study.

**Table 2:** Experimental results of terminal velocities of isolated bubbles generated in Newtonian (Water) and non-Newtonian (CMC and XG) solutions in a 4 mm gap column

Fluid	$d_{cap}$ (mm)	$d_b$ (mm)	Confinement ratio ( $d_b/e$ )	$V_t$ (m/s) (confined)	$V_t$ (m/s) (non-confined)	$V_t$ Ratio (confined/non- confined)	Re	Re <sub>conf</sub>	Eo	C <sub>D</sub>
Water					<i>Jamialahmadi et al. (1994)</i>					
	0.127	1.74	0.435	0.1948	0.3139	0.620	339		0.408	0.600
	0.254	1.95	0.4875	0.2014	0.3001	0.671	393		0.512	0.629
	0.508	2.78	0.695	0.1853	0.2619	0.707	515		1.041	1.059
	0.762	3.12	0.78	0.1704	0.2545	0.669	536		1.312	1.384
	1.016	3.28	0.82	0.2030	0.2505	0.810	666		1.450	1.041
CMC (2 g·L <sup>-1</sup> )					<i>Margaritis et al. (1999)</i>					
	0.127	1.58	0.395	0.1301			15.92	17.48	0.364	1.221
	0.254	2.22	0.555	0.1797			30.71	42.33	0.718	0.899
	0.508	2.82	0.705	0.1876			38.02	65.84	1.159	1.048
	0.762	3.16	0.79	0.1883			41.14	83.54	1.455	1.166
	1.016	3.28	0.82	0.1890			42.36	92.00	1.568	1.201
XG (1 g·L <sup>-1</sup> )	0.127	1.34	0.335	0.0800	0.0596	1.342	6.33	6.36	0.339	2.739
	0.254	2.2	0.55	0.1587	0.1265	1.254	23.11	39.65	0.914	1.143
	0.508	3.1	0.775	0.1621	0.1765	0.918	27.38	87.85	1.814	1.543
	0.762	3.14	0.785	0.1647	0.1985	0.829	28.23	93.82	1.861	1.514
	1.016	3.36	0.84	0.1594	0.2205	0.722	27.60	114.22	2.131	1.723

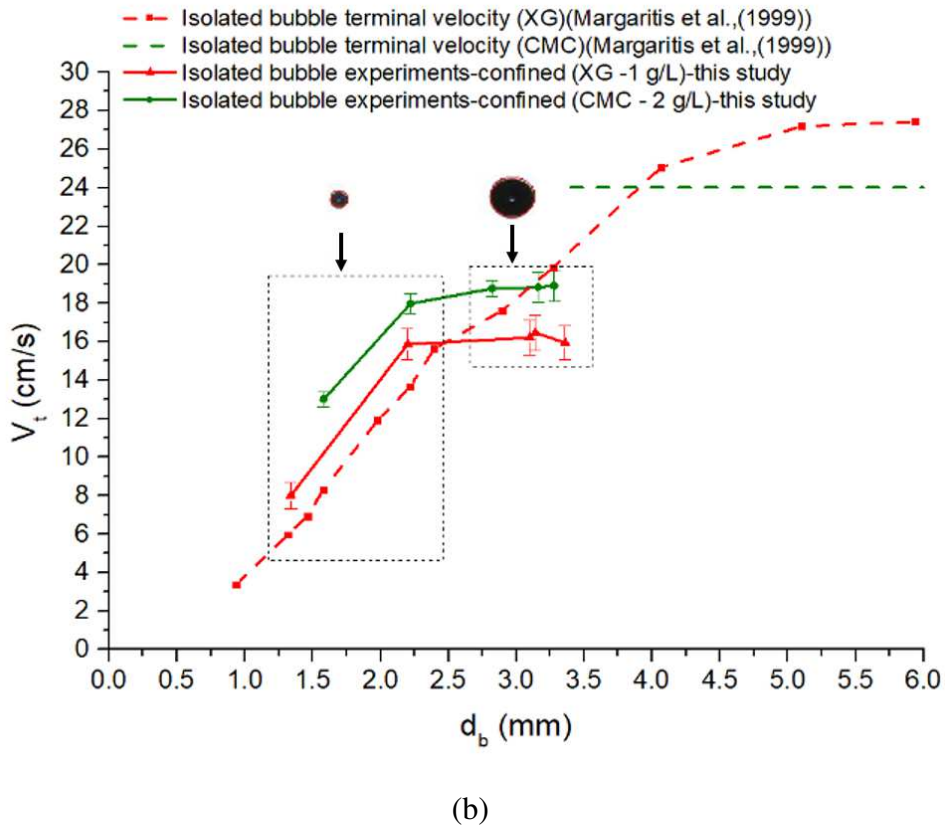
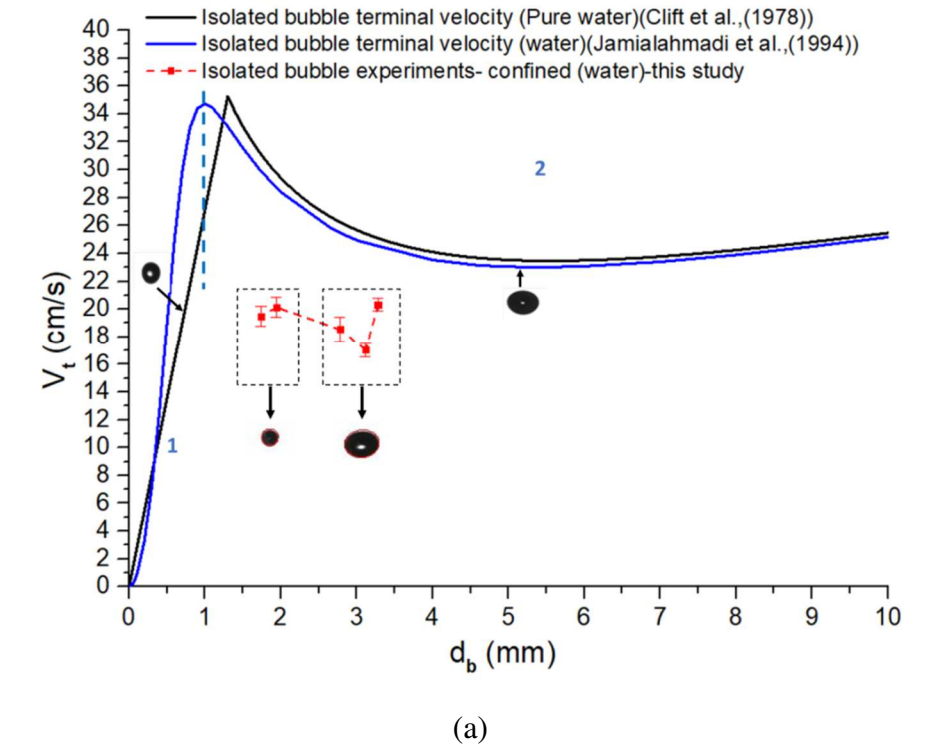


**Figure 3:** Terminal velocity of isolated bubbles vs diameter. (a) demineralized water: comparison between results in a thin-gap column (present study) and literature ones: Jamialahmadi et al. (1994) and Clift et al. (1978) for unconfined bubbles. (b) CMC and XG solutions: comparison between results in confined environment (present study) and in infinite medium: Margaritis et al., 1999

## 3.2. Shape and trajectory of isolated bubbles in 2D confined conditions

### 3.2.1. Shape of isolated bubbles in 2D confined conditions

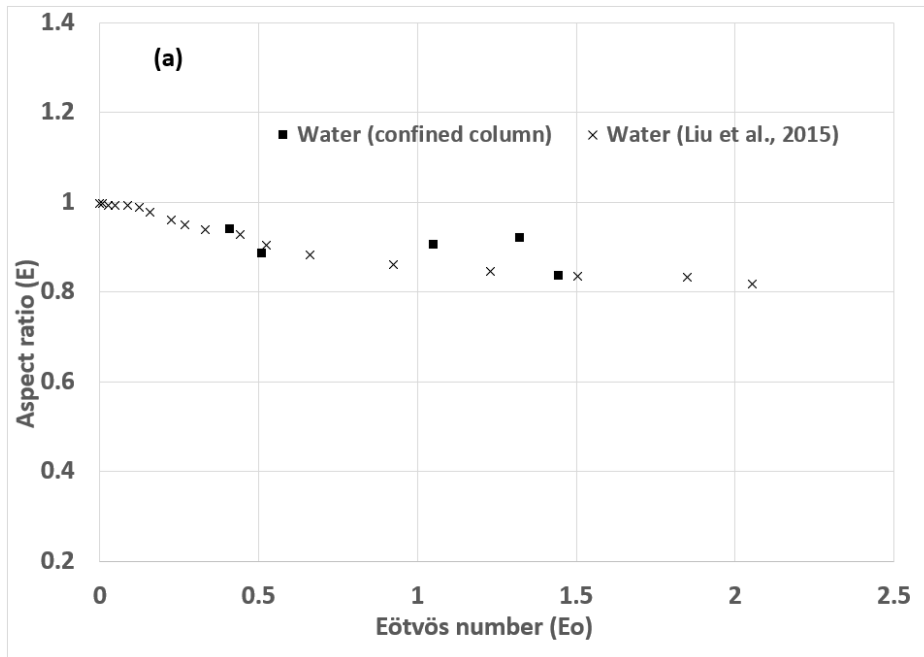
The evolution of the bubbles shape in water vs bubble diameter based on the Grace diagram – giving the bubble shape and velocity as a function of the Reynolds, Eötvös and Morton dimensionless numbers (Grace et al., 1976)- is shown in Figure 3(a). According to this diagram (Clift et al., 1978), the classic evolution of the bubble shape for gravitational motion in water and for infinite medium is described in 3 domains: (1) small bubbles with low terminal velocity that behave like rigid spheres, (2) bubbles which can no longer be assimilated to spheres, their shape gradually passing to ellipsoids, (3) when the diameter increases, the ellipsoid becomes a spherical cap (not shown here). In the present study, shadowgraphy analysis shows a shift in this evolution for the confined geometry, with the persistence of the spherical shape regime at larger diameters: up to 2 mm whereas the transition between spherical and ellipsoidal regimes occurs at around 1 mm for pure water in unconfined conditions (Figure 3(a)).

For the shear-thinning XG and CMC solutions, two shape categories are observed (Figure 3(b)). In the creeping flow regime, rigid spheres are observed. From bubble diameter greater or equal than 3 mm and the plateau zone of the terminal velocity, the oblate ellipsoid shape is observed.

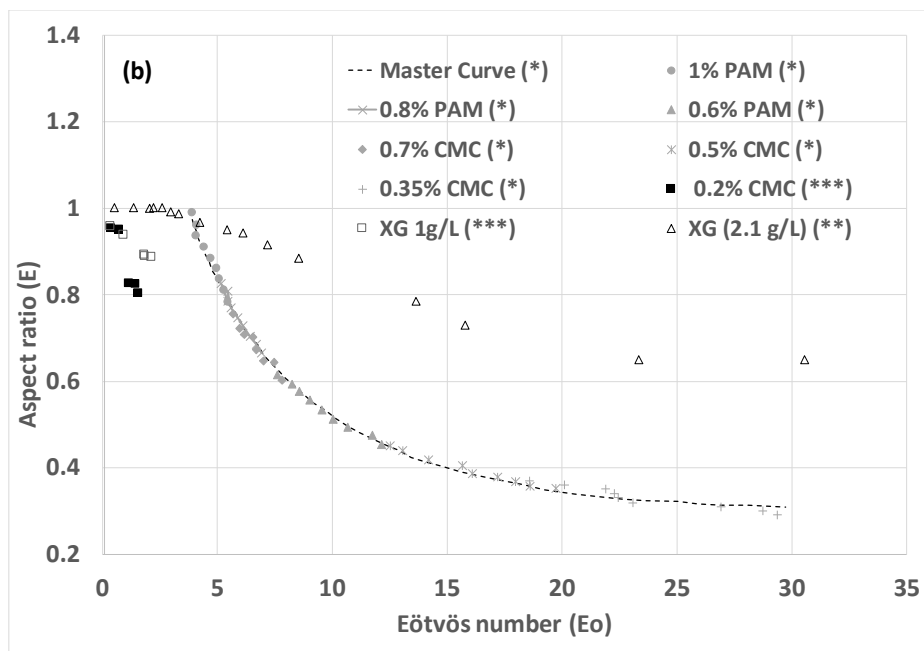
Considering spherical or ellipsoidal bubbles, the aspect ratio  $E$  (ratio between the equivalent diameter and maximal horizontal diameter) is used in this study to characterize the bubble shape. In Figure 4, the comparison of this factor vs Eötvös number ( $E_o$ ) is carried out for the three tested solutions. Experimental results of Liu et al. (2015), Fan et al. (2010) and Amirnia

et al. (2013) are plotted in order to compare the present results to those of an unconfined medium.

In water, as shown in Figure 4(a), for small  $Eo$  numbers ( $Eo < 0.5$ ), spherical bubbles with  $E$  values close to one are first observed as in unconfined conditions (Liu et al., 2015). Then, for  $Eo$  between 1 and 1.3, the aspect ratio in the confined column is higher than in infinite medium: as already observed visually, deformation of the bubble with increasing  $Eo$  number or equivalent diameter is delayed in confined conditions. For the highest  $Eo$  value ( $Eo = 1.45$ ), the aspect ratio is similar to the one obtained by Liu et al. (2015). In non-Newtonian solutions, Fan et al. (2010) have shown that the  $E$  ratio decreases gradually with the increase in  $Eo$  parameter according to the master curve presented in Figure 4(b) which is based on results with both CMC and polyacrylamide (PAM) solutions of various concentrations. In confined conditions, the same evolution of  $E$  is observed in the CMC solution but the decrease is observed for smaller  $Eo$  numbers, corresponding to smaller bubble diameters. The same remark is valid for the XG solution when the results in the confined column are compared to those of Amirnia et al. (2013) despite the difference in the concentration (XG at  $2.1 \text{ g}\cdot\text{L}^{-1}$  in Amirnia et al. (2013)). Therefore, for bubbles rising in shear-thinning fluids, contrary to water, confinement induces a transition from spherical shape to ellipsoidal shape that occurs sooner in terms of bubbles diameter or  $Eo$  number.



(a)



(b)

**Figure 4:** Aspect ratio ( $E$ ) of air bubbles in different solutions plotted as a function of Eötvös number ( $E_o$ ). (a) air – water. (b) air - non-Newtonian solutions.

(\*) Fan et al. ; (\*\*) Amirnia et al, (\*\*\*) confined column, present study

### 3.2.2. Trajectory of isolated bubbles in 2D confined conditions

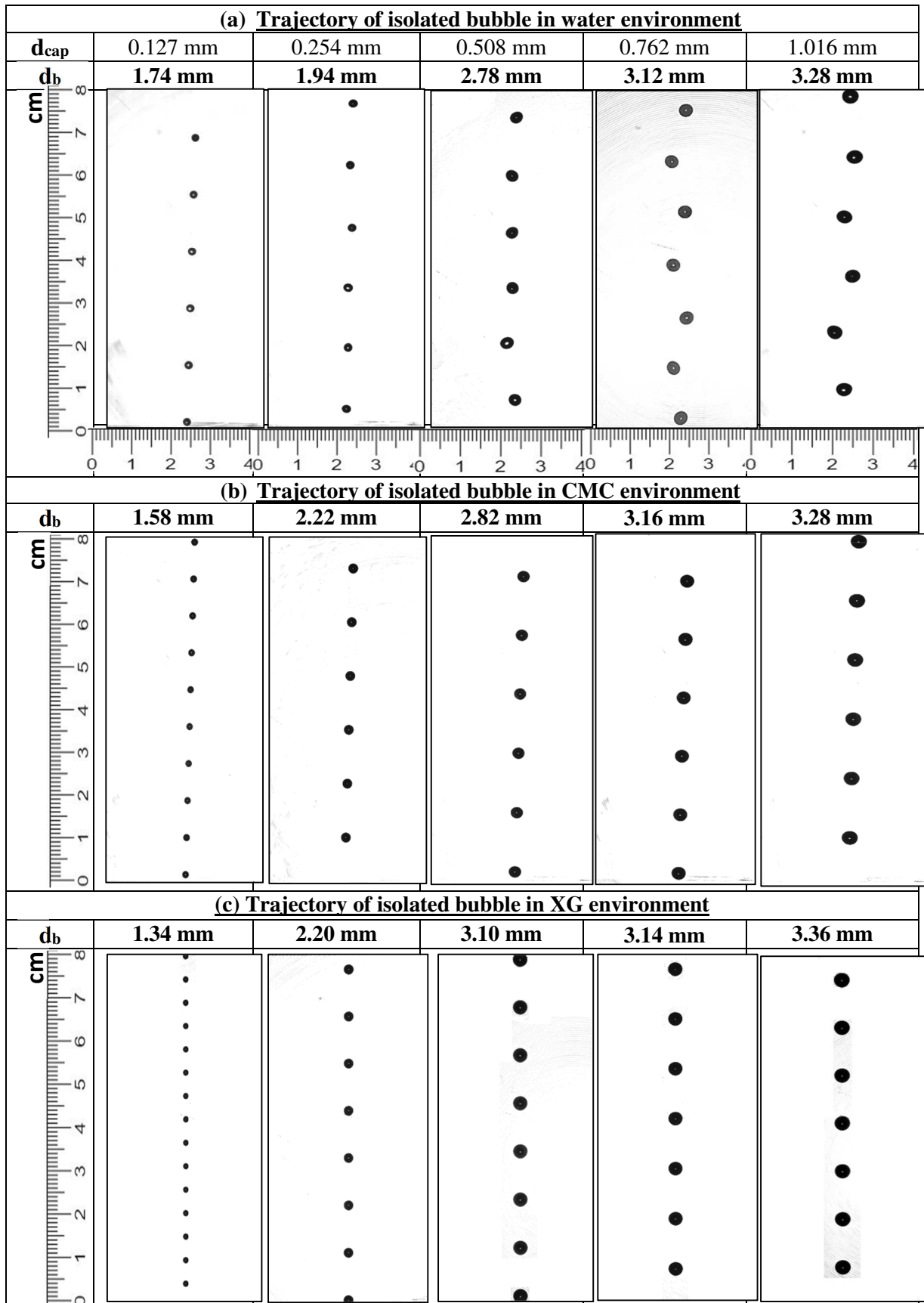


**Figure 5:** Instantaneous images in the plane of the 2D column of bubble rising in water (a), CMC solution (b) and XG solution (c) for the different bubble diameters (Frequency between 2 bubble images = 15 Hz)

Trajectory and shape of bubbles are important factors that influence gas-liquid mass transfer, wall shear stress and mixing in bubbly flows. Figure 5 shows these two parameters for water, CMC and XG solutions and different bubble diameters. For air-water system, the passage from the rectilinear trajectory towards an oscillating one is observed when the bubble shape becomes ellipsoidal. In this oscillating regime, the viscosity forces have no effect on the rise of the bubble compared to the surface tension forces. For the CMC and the XG solutions, the viscosity forces are very important, therefore the trajectory remains rectilinear whatever the diameter of the bubbles. The oscillation along a zigzag path observed in air-water system leads to periodic inclinations of the ellipsoidal bubbles, whereas in the case of CMC and XG solutions the rectilinear trajectory imposes an oblate ellipsoid shape with a fixed horizontal major axis.

The oscillating behavior of bubbles is also characterized using the fluctuating components of the horizontal (u) and vertical (v) velocities according to the following equations:

$$\sqrt{\overline{u'^2}} = \sqrt{\frac{1}{n} \sum_{i=1}^n (u_i(t) - \bar{U})^2} \quad (3)$$

$$\sqrt{\overline{v'^2}} = \sqrt{\frac{1}{n} \sum_{i=1}^n (v_i(t) - \bar{V})^2} \quad (4)$$

Where  $u_i(t)$  and  $v_i(t)$  are the horizontal and vertical instantaneous velocities of single bubbles;  $\bar{U}$  and  $\bar{V}$  the average components ;  $v'$  and  $u'$  the fluctuating ones.

Figure 6 shows that for the vertical and the horizontal velocity components, fluctuations are about 50% greater with water than with CMC and XG solutions. For the horizontal component, a dependence on the diameter of the bubble is observed, with an increase in

fluctuations when the diameter increases, whereas the vertical component oscillations remain quite constant with the bubble diameter. Otherwise, the difference of fluctuations of the horizontal velocities between water and the two solutions of CMC and XG increases with the diameter.

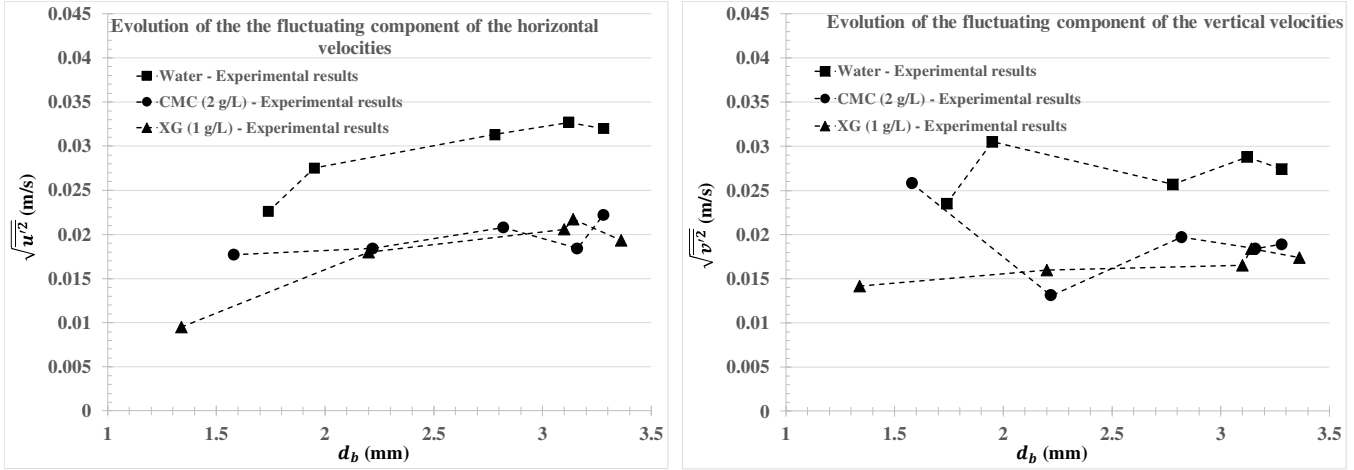


**Figure 6:** Horizontal and vertical velocity fluctuations vs bubble diameter for water, CMC and XG solutions

### 3.3. Dimensional analysis and correlation of drag coefficient

First, the case of water will be discussed and then the more complex case of shear-thinning fluids where confinement both increases the wall friction but also reduces the liquid viscosity around the bubble will be more deeply investigated.

#### a. Water

The drag coefficient  $C_D = \frac{4gd_b}{3V_t^2}$  in our confined conditions is plotted as a function of the bubble Reynolds number in Figure 7. In the same figure, the drag coefficient in unconfined conditions (infinite liquid medium)  $C_{Dinf}$  coming from the correlation of Jamialahmadi et al.(1994) is presented:

$$V_t = \frac{V_{bs}V_{bw}}{\sqrt{V_{bs}^2 + V_{bw}^2}} \quad (5)$$

where 
$$V_{bs} = \frac{1}{18} \frac{\rho_L - \rho_G}{\mu_L} g d_b^2 \frac{3\mu_L + 3\mu_G}{2\mu_L + 3\mu_G} \quad V_{bw} = \sqrt{\frac{2\sigma}{d_b(\rho_L + \rho_G)} + \frac{g d_b}{2}}$$

The same evolution of  $C_D$  with  $Re$  as in unconfined conditions is observed, but with a much higher value, which is coherent with the conclusions already made for the terminal velocity in water which is significantly decreased by confinement due to wall friction.

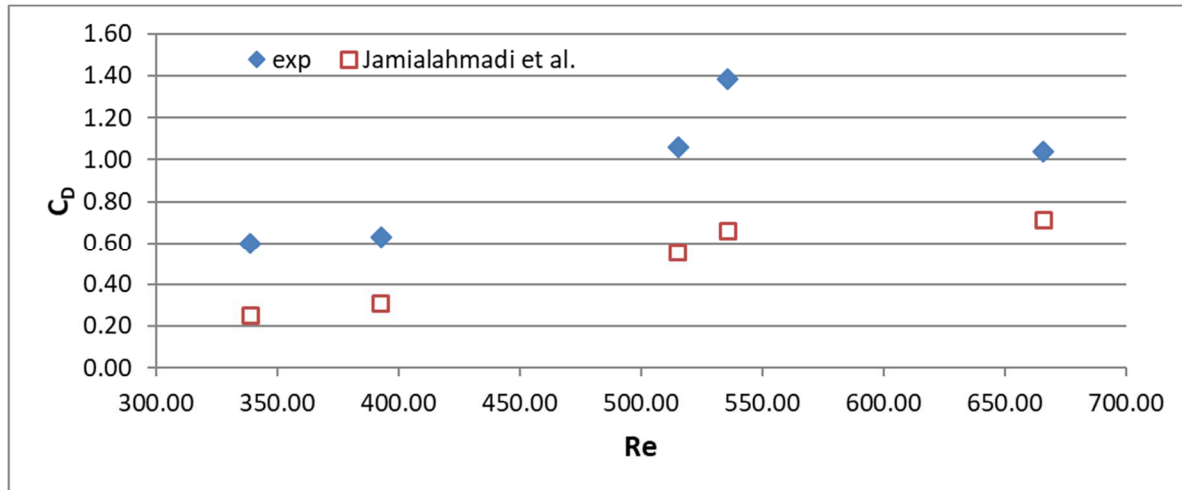


**Figure 7:** Drag coefficient as a function of Reynolds number for water as the liquid phase and comparison with unconfined conditions

The influence of confinement on the  $C_D/C_{Dinf}$  ratio has been investigated by Figueroa-Espinoza et al.(2008). They showed a strong influence of confinement on  $C_D$ . They verified that, when the inertial effects dominate, which is obtained for  $Re > 100$ ,  $C_D/ C_{Dinf} = 1 + 80 s^3$  where  $s = d_b / (2e)$  *i.e.*  $C_D/ C_{Dinf} = 1 + 10 (d_b / e)^3$ . This relation is plotted in Figure 8, as well as the values obtained in the present study: it can be observed that they are very close for  $d_b/e \leq 0.5$  and then the experimental values do no longer follow the 3<sup>rd</sup> order polynomial tendency but remain quite constant. It must be noticed, that if the study of Figueroa-Espinoza et al. (2008) covers the same range of confinement ratio as the present one, it is limited to  $Re < 500$  whereas our experimental values for  $d_b/e > 0.5$  correspond to  $Re > 500$ . This may explain why the present results do not follow the extrapolation of the correlation established by these authors. A more complete experimental study should be carried out to verify if another

correlation should be used to assess the effect of confinement on the drag coefficient at Reynolds numbers higher than 500.

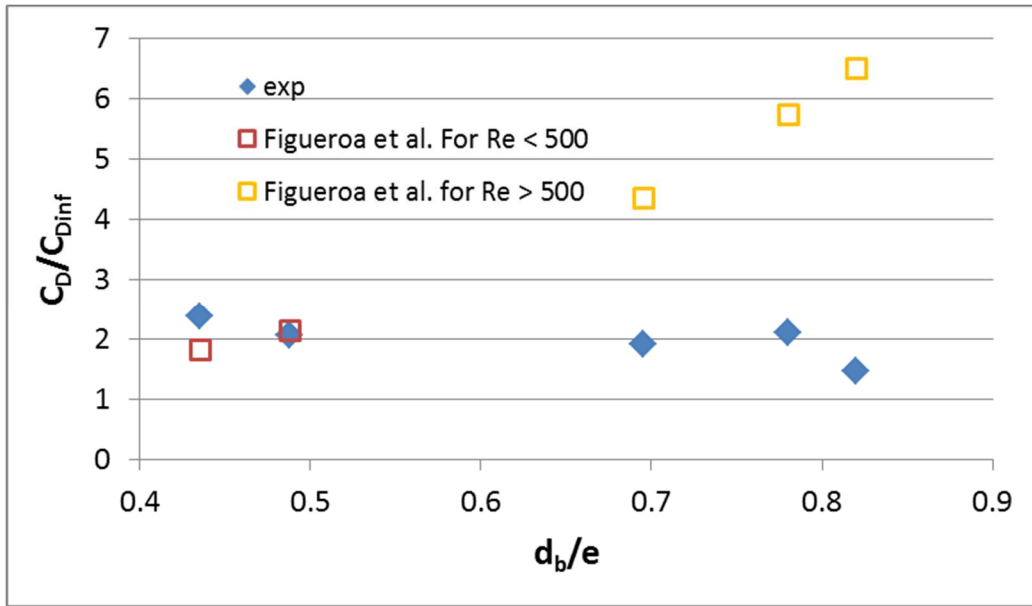


**Figure 8:**  $C_D / C_{Dinf}$  as a function of the confinement ratio  $d_b/e$  for water as the liquid phase and comparison with the relation of Figueroa-Espinoza et al. (2008)

*b. Shear-thinning fluids*

Margaritis et al.(1999) established the following correlation for  $C_D$  in power law fluids **and infinite liquid:**

$$C_D = \frac{16}{Re} (1 + 0.173 Re^{0.657}) + \frac{0.413}{1+16300Re^{-1.09}} \quad \text{for } Re < 60 \quad (6a)$$

$$C_D = 0.95 \quad \text{for } Re > 60 \quad (6b)$$

where, for bubbles rising in power law fluids, the apparent viscosity is estimated using the average shear-rate over the bubble surface:  $V_t/d_b$ , which gives:

$$\mu_a = K \left( \frac{V_t}{d_b} \right)^{n-1} \quad (7)$$

and thus

$$Re = \frac{\rho_L d_b^n V_t^{2-n}}{K} \quad (8)$$

Figure 9(a) compares the  $C_D$  values obtained in the CMC and XG solutions in the confined column to the ones predicted by the Margaritis *et al.* correlation. It can be observed that no clear link seems to exist between the values of  $C_D$  in confined and unconfined conditions and that the evolution of the drag coefficient with  $Re$  in confined conditions follows no clear tendency.

In fact, the definition of the apparent viscosity for bubbles rising in an infinite liquid medium does not reflect the fact that in confined conditions, when the bubble diameter increases, the confinement ratio increases as well as the shear rate around the bubble, therefore the apparent viscosity decreases. That is why, we define here a “confined Reynolds number” where the apparent viscosity is defined using the shear rate between the wall and the bubble:

$$\dot{\gamma} = \frac{V_t}{1/2(e-d_b)} \quad (9)$$

This definition is valid only for slightly confined bubbles ( $e > d_b$ ) as in the present study:  $d_b/e < 1$

With this definition, the apparent viscosity of power law fluids is defined as:

$$\mu_{app} = K \left( \frac{2V_t}{e-d_b} \right)^{n-1} \quad (10)$$

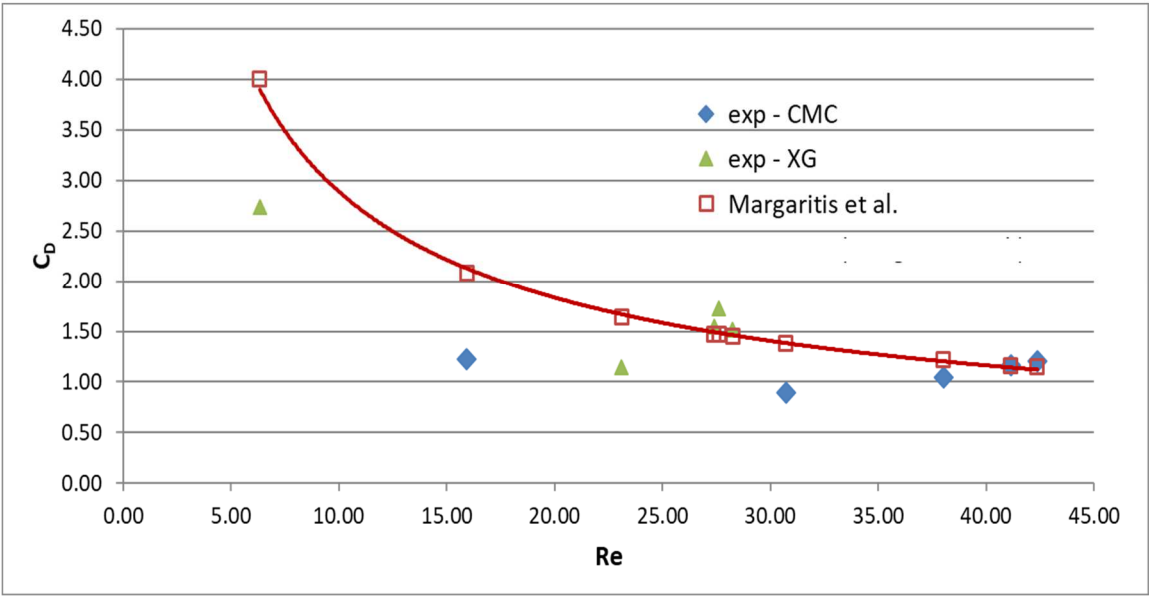
and the confined Reynolds number as:

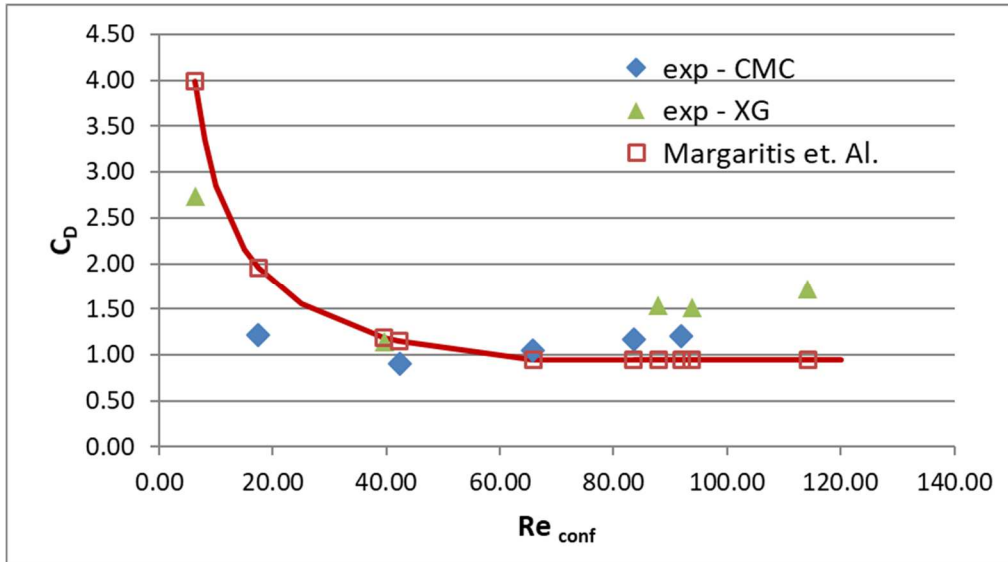
$$Re_{conf} = \frac{\rho_L d_b (e-d_b)^{n-1} V_t^{2-n}}{K 2^{n-1}} \quad (11)$$

Figure 9(b) compares the experimental values of  $C_D$  to the correlation of Margaritis *et al.* when the Reynolds number is calculated as the confined Reynolds number. In that figure, it can be seen that Margaritis *et al.* correlation using the new Reynolds definition still cannot

describe the drag coefficient evolution but it can also be seen that a clear tendency of the evolution of  $C_D$  with  $Re_{conf}$  is observed: a decrease, followed by an increase at higher Reynolds numbers.

The experimental values of  $C_D$  appear to be smaller than the ones predicted by the Margaritis *et al.* correlation at low  $Re$  numbers, these cases correspond to the smallest bubble diameters and low confinement ratio: in that case, the viscosity reduction outweighs the wall friction effect. But at high  $Re$  numbers, the experimental values of  $C_D$  are larger than the ones predicted by the correlation of Margaritis, which is explained by the wall friction effect which is more important than the one of viscosity reduction. It can be concluded that Margaritis *et al.* correlation using a modified Reynolds number to take into account the effect of confinement on the apparent viscosity cannot represent the drag coefficient in confined conditions. A new correlation has to be established which takes into account the confinement ratio  $d_b/e$ .





**Figure 9:**

- (a) Experimental drag coefficient for shear-thinning fluids in confined conditions as a function of  $Re$ , comparison with the correlation of Margaritis et al.
- (b) Experimental drag coefficient for shear-thinning fluids in confined conditions as a function of  $Re_{conf}$  (confined Reynolds number), comparison with the correlation of Margaritis et al.

To develop this correlation, the Buckingham's Pi theorem is applied. The terminal velocity depends on the liquid properties, on the bubble characteristics, on the gravity acceleration and on the column gap:

$$V_t = f(\rho_L, \mu_L(K, n), \sigma, d_b, g, e) \quad (12)$$

Application of Buckingham's Pi theorem allows to represent the above relation with four dimensionless numbers:

$$C_D = f(Re_{conf}, Eo, d_b/e) = A Re_{conf}^B Eo^C \left(\frac{d_b}{e}\right)^D \quad (13)$$

Coefficients A, B, C and D are obtained using the least square method giving:

$$C_D = 106.4 Re_{conf}^{-1.125} Eo^{1.395} \left(\frac{d_b}{e}\right)^{0.07} \quad (14)$$

Figure 10 compares the experimental values of  $C_D$  to this dimensionless correlation showing that the experimental results can be predicted by this correlation in a satisfying manner (error below 25%).

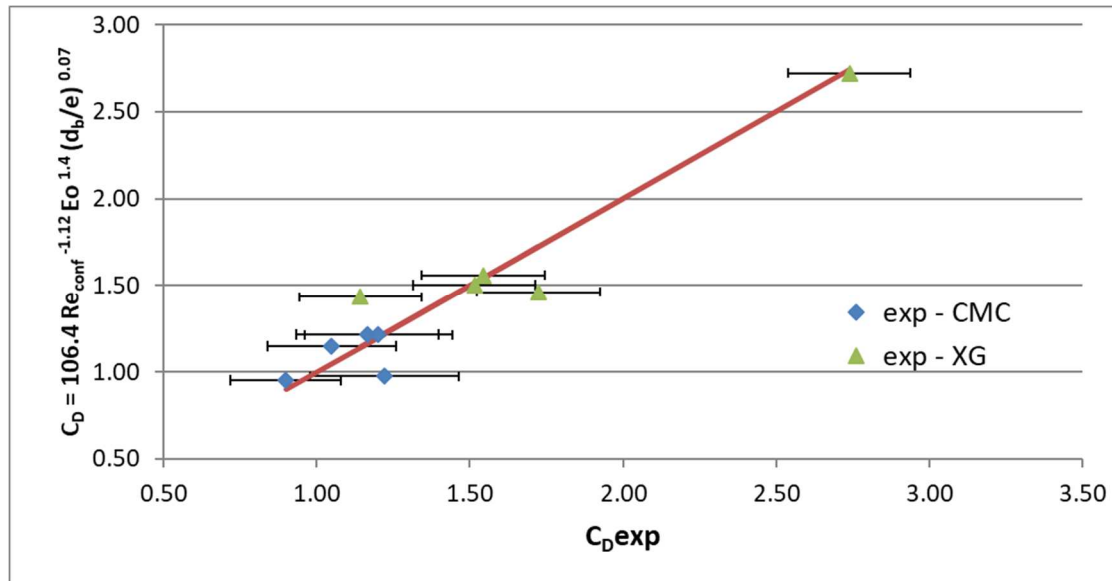


**Figure 10:** Comparison between experimental drag coefficient and the proposed correlation for shear-thinning fluids in confined conditions.

#### 4. Conclusion and perspectives

This study investigated experimentally the terminal velocity, shape and trajectory of bubbles of different diameters rising in a 4 mm-gap bubble column containing either Newtonian or non-Newtonian fluids. The roles of shear-thinning behavior of the liquid phase, as well as confinement have been put into evidence.

In particular, confinement logically reduces bubble terminal velocity in Newtonian fluids due to increased wall friction. But, for non-Newtonian fluids, it has been shown that confinement can induce either lower or higher terminal velocities than in unconfined geometries, depending on the confinement ratio because of antagonistic effects of increased wall friction

and decrease of viscosity with the shear-rate. This behavior can have important consequences in the context of high concentration microalgae cultivation since bubble terminal velocity will impact bubbles residence time in the bioreactor, as well as contact time with the liquid. This will have consequences on the collision probability in the reactor and therefore on coalescence frequency and interfacial area and on gas-liquid mass transfer  $k_L$  coefficient. Thus at the scale of the reactor, for PBRs operating at concentrations leading to non-Newtonian behavior of the liquid phase, confinement ratio by controlling either the column gap or the bubble diameter at sparger should have to be taken into account to ensure sufficient gas-liquid mass transfer rate. **In particular, the domain where confinement allows an increase of the terminal velocity compared to an infinite medium seems promising since according to Higbie's model (Higbie, 1935) for  $k_L$ , gas-liquid mass transfer diminishes with the contact time between the bubble and the liquid *i.e.* increases with the relative velocity:**

$$k_L = 2 * \sqrt{\frac{D_L}{\pi * t_{exp}}} \quad (15)$$

**In that case, the shear-thinning effect in confined conditions could partially compensate the effect of increased viscosity which deteriorates mass transfer (Thobie et al., 2017). Another study is currently carried out on the hydrodynamics of the whole bubble column in the presence of a swarm of bubbles generated by uniform sparging. The influence of bubble size at sparger is studied by using different capillary diameters. Several flowrates are investigated to characterize the homogeneous, transition and heterogeneous regimes and the link with the phenomena at the bubble scale characterized is established**

This paper also investigated the shape of bubbles in confined conditions, showing a transition from spherical to ellipsoidal regimes as a function of the diameter or Eo number, which occurs later in water and sooner in shear-thinning fluids compared to the case of infinite liquid medium.

Finally, a correlation for the drag coefficient in thin-gap bubble columns with confinement ratios between 0.34 and 0.84 and a shear-thinning liquid phase described by a power law is proposed. Further steps will be to study the case of a bubble swarm in the same conditions via shadowgraphy technique, as well as to characterize the global hydrodynamics (gas retention, mixing time) and gas-liquid mass transfer.

### Acknowledgments

The authors would like to gratefully acknowledge the financial support from the Higher Education Commission (HEC), Pakistan and also to Campus France for the kind cooperation in Sikandar ALMANI's Ph.D.

### Nomenclature

$C_D$		drag coefficient
$C_{Dinf}$		bubble drag coefficient in infinite liquid medium
$d_b$	(m)	bubble equivalent diameter
$d_{cap}$	(m)	capillary diameter
$e$	(m)	gap width
$E$		bubble aspect ratio
$Eo$		Eötvös Number
$Mo$		Morton number
$Re$		Reynolds Number
$Re_{conf}$		Reynolds Number in confined conditions
$u, v$	( $m.s^{-1}$ )	horizontal and vertical components of the bubble velocity
$u', v'$	( $m.s^{-1}$ )	horizontal and vertical fluctuating components of the bubble velocity
$\bar{U}, \bar{V}$	( $m.s^{-1}$ )	horizontal and vertical average velocities
$V_t$	( $m.s^{-1}$ )	bubble terminal velocity

$g$	(m. s <sup>-2</sup> )	gravitational acceleration
$K$		power law consistency index
$n$		power law flow index

#### Greek letters

$\dot{\gamma}$	(s <sup>-1</sup> )	shear rate
$\mu_{app}$	(Pa.s)	apparent viscosity
$\mu_L$	(Pa.s)	viscosity of the liquid phase
$\mu_G$	(Pa.s)	viscosity of the gas phase
$\rho_L$	(kg.m <sup>-3</sup> )	density of the liquid phase
$\rho_G$	(kg.m <sup>-3</sup> )	density of the gas phase
$\sigma$	(N.m)	surface tension
$\tau$	(Pa)	shear stress

#### **References:**

- Adesanya, V.O., Vadillo, D.C., Mackley, M.R., 2012. The rheological characterization of algae suspensions for the production of biofuels. *Journal Rheol.* 56, 925–939. <https://doi.org/10.1122/1.4717494>
- Akita, K., Yoshida, F., 1973. Gas holdup and volumetric mass transfer coefficient in bubble columns- Effects of liquid properties. *Ind. Eng. Chem. Process Des. Dev.* 12, 76–80. <https://doi.org/10.1021/i260045a015>
- Amirnia, S., de Bruyn, J.R., Bergougnou, M.A., Margaritis, A., 2013. Continuous rise velocity of air bubbles in non-Newtonian biopolymer solutions. *Chem. Eng. Sci.* 94, 60–68. <https://doi.org/10.1016/j.ces.2013.02.032>
- Böhm, L., Brehmer, M., Kraume, M., 2016. Comparison of the single bubble ascent in a Newtonian and a Non-Newtonian liquid: A phenomenological PIV study. *Chemie-Ingenieur-Technik* 88, 93–106. <https://doi.org/10.1002/cite.201500105>
- Böhm, L., Drews, A., Kraume, M., 2013. Bubble induced shear stress in flat sheet membrane systems—Serial examination of single bubble experiments with the electrodiffusion method. *J. Memb. Sci.* 437, 131–140. <https://doi.org/10.1016/j.memsci.2013.02.036>
- Böhm, L., Kurita, T., Kimura, K., Kraume, M., 2014. Rising behaviour of single bubbles in

- narrow rectangular channels in Newtonian and non-Newtonian liquids. *Int. J. Multiph. Flow* 65, 11–23. <https://doi.org/10.1016/j.ijmultiphaseflow.2014.05.001>
- Chhabra, R.P., 2006. *Bubbles, Drops, and Particles in Non-Newtonian Fluids*, Second Edi. ed. CRC press.
- Clift, R., Grace, J.R., Weber, M.E., 1978. *Bubbles, drops and particles*, Academic Press. Academic Press, NY.
- Dewsbury, K., Karamanev, D., Margaritis, A., 1999. Hydrodynamic characteristics of free rise of light solid particles and gas bubbles in non-Newtonian liquids. *Chem. Eng. Sci.* 54, 4825–4830. [https://doi.org/10.1016/S0009-2509\(99\)00200-6](https://doi.org/10.1016/S0009-2509(99)00200-6)
- Esmaeili, A., Guy, C., Chaouki, J., 2015. The effects of liquid phase rheology on the hydrodynamics of a gas – liquid bubble column reactor. *Chem. Eng. Sci.* 129, 193–207. <https://doi.org/10.1016/j.ces.2015.01.071>
- Fan, W., Ma, Y., Jiang, S., Yang, K., Li, H., 2010. An experimental investigation for bubble rising in non-newtonian fluids and empirical correlation of drag coefficient. *J. Fluids Eng. Trans. ASME* 132, 021305-1-021305-7. <https://doi.org/10.1115/1.4000739>
- Fan, W., Sun, Y., Chen, H., 2014. Bubble volume and aspect ratio generated in non-Newtonian fluids. *Chem. Eng. Technol.* 37, 1566–1574. <https://doi.org/10.1002/ceat.201400083>
- Felis, F., Strassl, F., Laurini, L., Dietrich, N., Billet, A.M., Roig, V., Herres-Pawlis, S., Loubière, K., 2019. Using a bio-inspired copper complex to investigate reactive mass transfer around an oxygen bubble rising freely in a thin-gap cell. *Chem. Eng. Sci.* 207, 1256–1269. <https://doi.org/10.1016/j.ces.2019.07.045>
- Figueroa-Espinoza, B., Zenit, R., Legendre, D., 2008. The effect of confinement on the motion of a single clean bubble. *J. Fluid Mech.* 616, 419–443. <https://doi.org/10.1017/S0022112008004072>
- Filella, A., Ern, P., Roig, V., 2015. Oscillatory motion and wake of a bubble rising in a thin-gap cell. *J. Fluid Mech.* 778, 60–88. <https://doi.org/10.1017/jfm.2015.355>
- Fransolet, E., Crine, M., Marchot, P., Toye, D., 2005. Analysis of gas holdup in bubble columns with non-Newtonian fluid using electrical resistance tomography and dynamic gas disengagement technique. *Chem. Eng. Sci.* 60, 6118–6123. <https://doi.org/10.1016/j.ces.2005.03.046>
- Grace, J.R., Wairegi, T., Nguyen, T.H., 1976. Shapes and velocities of single drops and bubbles moving freely through immiscible liquids. *Trans. Instn. Chem. Engrs* 54, 167–173.

- Gumulya, M., Utikar, R.P., Pareek, V.K., Evans, G.M., Joshi, J.B., 2021. Dynamics of bubbles rising in pseudo-2D bubble column: Effect of confinement and inertia. *Chem. Eng. J.* 405, 126615. <https://doi.org/10.1016/j.cej.2020.126615>
- Hashida, M., Hayashi, K., Tomiyama, A., 2019. Rise velocities of single bubbles in a narrow channel between parallel flat plates. *Int. J. Multiph. Flow* 111, 285–293. <https://doi.org/10.1016/j.ijmultiphaseflow.2018.09.015>
- Higbie, R., 1935. The rate of absorption of a pure gas into still liquid during short periods of exposure. *Trans. Am. Inst. Chem. Eng.* 31, 365–389.
- Islam, M. T., Ganesan, P. B., Cheng, J., & Uddin, M.S., 2020. Single bubble rising behaviors in Newtonian and non-Newtonian fluids with validation of empirical correlations : A computational fluid dynamics study. *Engineering Reports*, 2(1), e12100. <https://doi.org/10.1002/eng2.12100>
- Jamialahmadi, M., Branch, C., Muller-Steinhagen, H., 1994. Terminal bubble rise velocity in liquids 72(A), 119–122.
- Jamshidi, N., Mostoufi, N., 2018. Investigating bubble dynamics in a bubble column containing shear thinning liquid using a dual-tip probe. *Exp. Therm. Fluid Sci.* 94, 34–48. <https://doi.org/10.1016/j.expthermflusci.2018.01.034>
- Kherbeche, A., Mei, M., Thoraval, M.J., Hébrard, G., Dietrich, N., 2020. Hydrodynamics and gas-liquid mass transfer around a confined sliding bubble. *Chem. Eng. J.* 386, 121461. <https://doi.org/10.1016/j.cej.2019.04.041>
- Kumar, P., Vanka, S.P., 2015. Effects of confinement on bubble dynamics in a square duct. *Int. J. Multiph. Flow* 77, 32–47. <https://doi.org/10.1016/j.ijmultiphaseflow.2015.06.014>
- Letzel, H.M., Schouten, J.C., Krishna, R., van den Bleek, C.M., 1999. Gas holdup and mass transfer in bubble column reactors operated at elevated pressure. *Chem. Eng. Sci.* 54, 2237–2246. [https://doi.org/10.1016/S0009-2509\(98\)00418-7](https://doi.org/10.1016/S0009-2509(98)00418-7)
- Liu, L., Yan, H., Zhao, G., 2015. Experimental studies on the shape and motion of air bubbles in viscous liquids. *Exp. Therm. Fluid Sci.* 62, 109–121. <https://doi.org/10.1016/j.expthermflusci.2014.11.018>
- Loubière, K., Hébrard, G., 2004. Influence of liquid surface tension (surfactants) on bubble formation at rigid and flexible orifices. *Chem. Eng. Process. Process Intensif.* 43, 1361–1369. <https://doi.org/10.1016/j.cep.2004.03.009>
- Margaritis, A., te Bokkel, D.W., Karamanev, D.G., 1999. Bubble rise velocities and drag coefficients in non-Newtonian polysaccharide solutions. *Biotechnol. Bioeng.* 64, 257–266. [https://doi.org/10.1002/\(SICI\)1097-0290\(19990805\)64:3<257::AID-](https://doi.org/10.1002/(SICI)1097-0290(19990805)64:3<257::AID-)

- Quemada, D., 1977. Rheology of concentrated disperse systems and minimum energy dissipation principle - I. Viscosity-concentration relationship. *Rheol. Acta* 16, 82–94. <https://doi.org/10.1007/BF01516932>
- Rafaï, S., Jibuti, L., Peyla, P., 2010. Effective viscosity of microswimmer suspensions. *Phys. Rev. Lett.* 104. <https://doi.org/10.1103/PhysRevLett.104.098102>
- Roig, V., Roudet, M., Risso, F., Billet, A.-M., 2012. Dynamics of a high-Reynolds-number bubble rising within a thin gap. *J. Fluid Mech.* 707, 444–466. <https://doi.org/10.1017/jfm.2012.289>
- Roudet, M., 2008. Hydrodynamique et transfert de masse autour d'une bulle confinée entre deux plaques. Thèse de Doctorat, Université de Toulouse.
- Roudet, M., Billet, A.M., Cazin, S., Risso, F., Roig, V., 2017. Experimental investigation of interfacial mass transfer mechanisms for a confined high-reynolds-number bubble rising in a thin gap. *AIChE J.* 63, 2394–2408. <https://doi.org/10.1002/aic.15562>
- Ruzicka, M.C., Drahoš, J., Fialová, M., Thomas, N.H., 2001. Effect of bubble column dimensions on flow regime transition. *Chem. Eng. Sci.* 56, 6117–6124. [https://doi.org/10.1016/S0009-2509\(01\)00215-9](https://doi.org/10.1016/S0009-2509(01)00215-9)
- Sharaf, S., Zednikova, M., Ruzicka, M.C., Azzopardi, B.J., 2016. Global and local hydrodynamics of bubble columns - Effect of gas distributor. *Chem. Eng. J.* 288, 489–504. <https://doi.org/10.1016/j.cej.2015.11.106>
- Souliès, A., 2014. Contribution à l'étude hydrodynamique et à la modélisation des photobioréacteurs à haute productivité volumique. Thèse de Doctorat, Université de Nantes.
- Souliès, A., Pruvost, J., Legrand, J., Castelain, C., Burghelca, T.I., 2013. Rheological properties of suspensions of the green microalga *Chlorella vulgaris* at various volume fractions. *Rheol. Acta* 52, 589–605. <https://doi.org/10.1007/s00397-013-0700-z>
- Thobie, C., Gadoin, E., Blel, W., Pruvost, J., Gentric, C., 2017. Global characterization of hydrodynamics and gas-liquid mass transfer in a thin-gap bubble column intended for microalgae cultivation. *Chem. Eng. Process. Process Intensif.* 122, 76–89. <https://doi.org/10.1016/j.cep.2017.10.009>
- van Sint Annaland, M., Deen, N.G., Kuipers, J.A.M., 2005. Numerical simulation of gas bubbles behaviour using a three-dimensional volume of fluid method. *Chem. Eng. Sci.* 60, 2999–3011. <https://doi.org/10.1016/j.ces.2005.01.031>
- Vial, C., Camarasa, E., Poncin, S., Wild, G., Midoux, N., Bouillard, J., 2000. Study of

hydrodynamic behaviour in bubble columns and external loop airlift reactors through analysis of pressure fluctuations. *Chem. Eng. Sci.* 55, 2957–2973.

[https://doi.org/10.1016/S0009-2509\(99\)00551-5](https://doi.org/10.1016/S0009-2509(99)00551-5)

Wileman, A., Ozkan, A., Berberoglu, H., 2012. Rheological properties of algae slurries for minimizing harvesting energy requirements in biofuel production. *Bioresour. Technol.* 104, 432–439. <https://doi.org/10.1016/j.biortech.2011.11.027>

Zhang, Z., Zhang, H., Yuan, X., Yu, K.T., 2020. Effective UV-Induced fluorescence method for investigating interphase mass transfer of single bubble rising in the Hele-Shaw cell. *Ind. Eng. Chem. Res.* 59, 6729–6740. <https://doi.org/10.1021/acs.iecr.9b07106>